Volume 11
Number 5
7 February 2023
Pages 1595–1996

Journal of Materials Chemistry C

Materials for optical, magnetic and electronic devices

rsc.li/materials-c

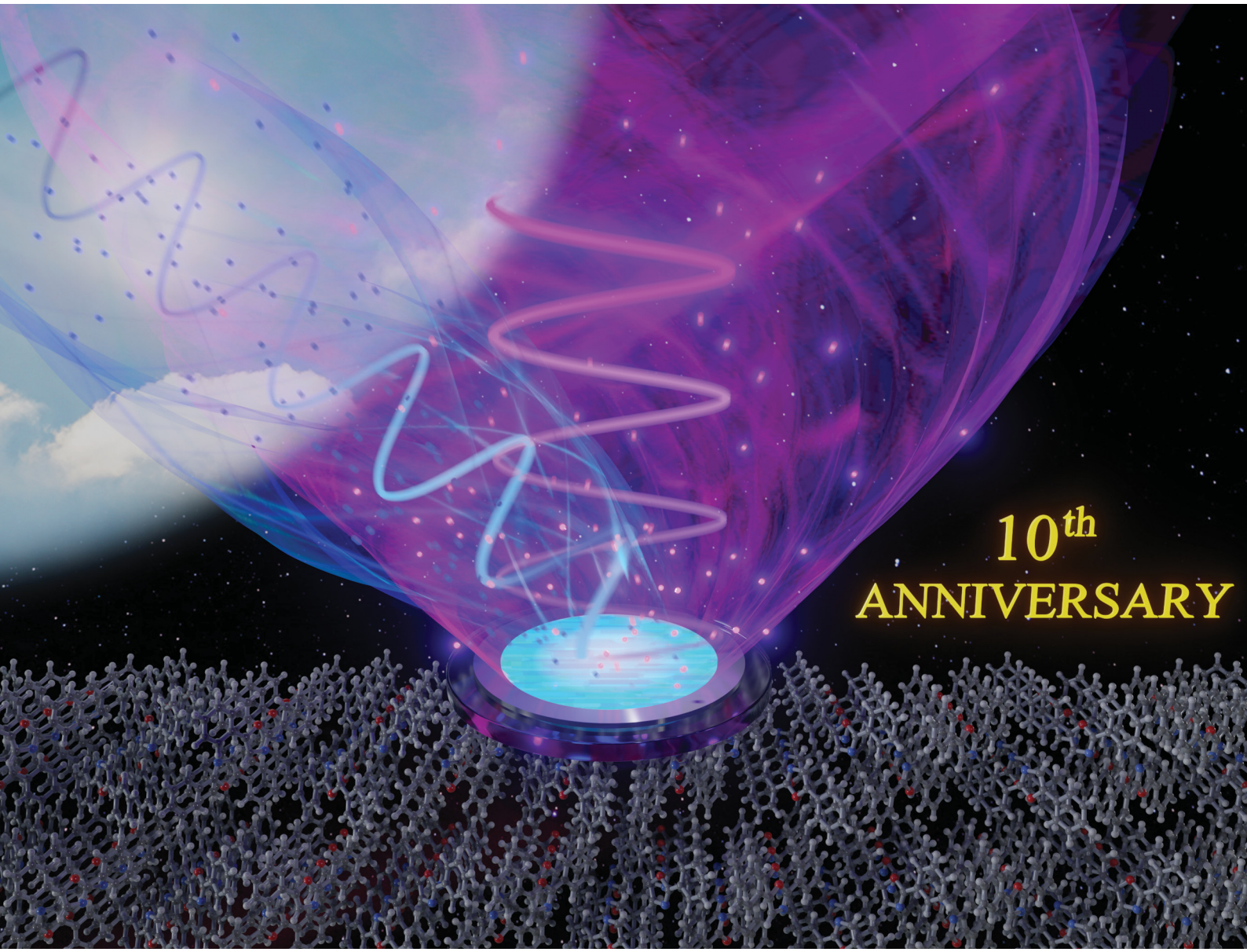

ISSN 2050-7526

ROYAL SOCIETY OF CHEMISTRY

COMMUNICATION

Riku Enomoto and Yoichi Murakami

Solvent-free temperature gradient melt formation of efficient visible-to-UV photon upconversion organic films with subsolar threshold and over 100 h photostability in air

10 YEARS ANNIVERSARY

Journal of Materials Chemistry C

ROYAL SOCIETY OF CHEMISTRY

COMMUNICATION

View Article Online
View Journal | View Issue

Cite this: J. Mater. Chem. C, 2023, 11, 1678

Received 27th October 2022,
Accepted 20th December 2022

DOI: 10.1039/d2tc04578h

rsc.li/materials-c

Solvent-free temperature gradient melt formation of efficient visible-to-UV photon upconversion organic films with subsolar threshold and over 100 h photostability in air†

Riku Enomoto [ab] and Yoichi Murakami *[ab]

Completely solvent-free "green" formation of bicomponent organic polycrystalline films for efficient visible-to-ultraviolet photon upconversion (UV–UC) were achieved by temperature-gradient solidification from the melt. The UV–UC film formed under optimal conditions exhibited an ultralow excitation threshold (0.3 suns, AM1.5 spectrum with a 413 nm long-pass filter) and a record-long photostability (>100 h) in air.

Ultraviolet (UV) light (wavelength < 400 nm) consisting of high-energy photons has broad utility; including photocatalytic generation of green hydrogen[1] and hydrocarbons,[2] photopolymerization,[3] and sanitization.[4] However, only *ca.* 4% of photons in terrestrial sunlight[5] constitute UV light, which has hindered efficient and effective uses of sunlight.

Photon upconversion (UC) based on triplet–triplet annihilation (TTA) (TTA-UC, Scheme 1) is an active area of research because of its potential of converting low-intensity light.[6,7] Since a visible-to-UV UC (UV–UC) was reported[8] in deaerated benzene by using biacetyl and 2,5-diphenyloxazole (PPO) as a metal-free sensitizer and annihilator, respectively, many UV–UCs in organic solvents have been reported;[8–12] although such systems generally exhibit photodegradation.[9] Recently, a photostability of 1 h was reported for UV–UCs in deaerated solvents with a UC quantum yield (Φ_{UC}) of *ca.* 10% or a normalized UC emission efficiency ($\eta_{UC} \equiv 2\Phi_{UC}$) of *ca.* 20%.[10,11] However, use of volatile, flammable, and bio-toxic solvents should be avoided for applications that usually demand safety, stability, and greenness. To date, after some early works that embedded chromophores into polymers,[13,14] solid-state UC has been intensively investigated.[15–18] However, no UV–UC solids with an excitation threshold comparable with or lower than terrestrial solar intensity have been reported.[14,18]

Recently, we developed van der Waals (vdW) solid–solution crystals of a hydrocarbon annihilator in which only 0.002 mol% of the porphyrin sensitizer was stably dissolved.[17] Although such slowly grown vdW crystals have afforded substantially high performance in air[17] and resolved the previous issue of low sample crystallinity,‡ the corresponding preparation used organic solvents during the recrystallization for 1–3 days.[17] Therefore, a solvent-free method to controllably and reproducibly generate high-performance UV–UC solids, preferably in the form of a film that is compatible with broad applications, is highly desired. Such a target would substantially impact our manner of using visible light and solve the problem of the low number of UV photons in sunlight.

Herein, we report completely solvent-free "green" formation of UV–UC solid thin films with outstanding high performance by using a temperature gradient controlled over a surface (Fig. 1a). This strategy, for the first time applied towards preparation of UC solids, enables formation of a bicomponent polycrystalline organic film from a melt of a sensitizer and an

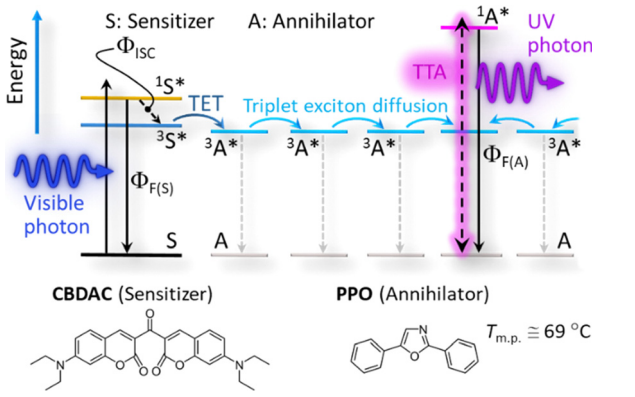

Scheme 1 Schematic energy diagram of TTA-UC in this study. X, ^{1}X*, and ^{3}X* (X = S: sensitizer or A: annihilator) denote the ground state, excited singlet state, and excited triplet state, respectively. TET: triplet energy transfer; TTA: triplet–triplet annihilation. Bottom shows the sensitizer and annihilator selected in this study.

[a] Laboratory for Zero-Carbon Energy, Institute of Innovative Research, Tokyo Institute of Technology, 2-12-1 Ookayama, Meguro-ku, Tokyo 152-8550, Japan. E-mail: murakami.y.af@m.titech.ac.jp
[b] Department of Mechanical Engineering, Tokyo Institute of Technology, 2-12-1 Ookayama, Meguro-ku, Tokyo 152-8552, Japan

† Electronic supplementary information (ESI) available. See DOI: https://doi.org/10.1039/d2tc04578h

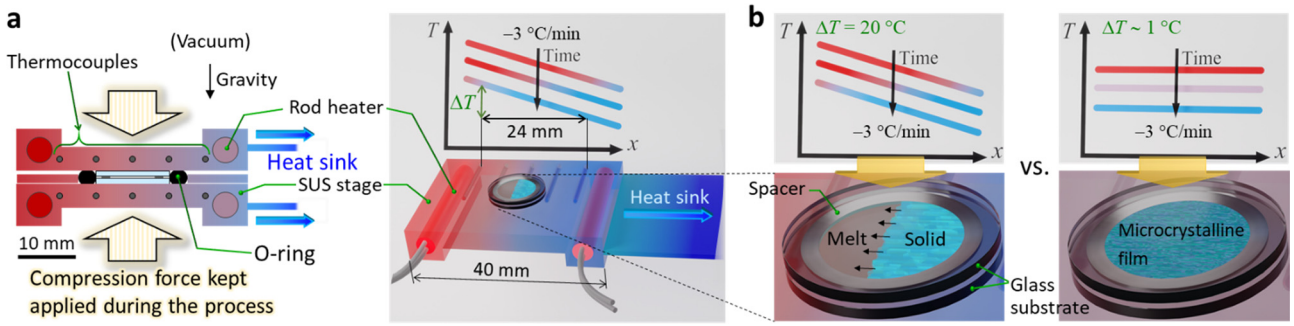

Fig. 1 Schematic of thin film formation under a controlled temperature gradient. (a) The apparatus developed for this study. The same temperature gradients were formed over two SUS stages, which sandwiches a stack of substrate–{PPO & CBDAC blend}–substrate set inside an O-ring. The temperature gradient was established by using two independently controlled rod heaters. Each stage has five thermocouples embedded at equal intervals (6 mm) and a heat sink attached to the one end. Right top describes the linear descent of the temperature profile and definition of ΔT. (b) Schematic of the difference in the results for the cases of ΔT = 20 °C *vs.* ~ 1 °C.

annihilator blend. Our investigations of this concept reveal an essential importance of optimizing the temperature gradient or cooling rate (Fig. 1b). Consequently, the UC film formed under optimal conditions exhibited a high Φ_{UC} = 4.3% (η_{UC} = 8.6%), substantially low excitation threshold (*ca.* 0.3× that of natural sunlight intensity), and record-long (>100 h) photostability ever reported for TTA–UC, all of which were achieved in air, as follows.

After our initial search for a suitable combination of the sensitizer and annihilator (some examples shown in Table S1, ESI†), we selected 3,3′-carbonylbis(7-diethylaminocoumarin) (CBDAC)[11,19,20] as the sensitizer and PPO as the annihilator (Scheme 1). CBDAC has a high intersystem-crossing quantum yield ($\Phi_{ISC} \cong$ 92%, in benzene),[19] whereas PPO has a low melting point ($T_{m.p.} \cong$ 69 °C, Fig. S6a, ESI†) and a high fluorescence quantum yield ($\Phi_{F(A)} \cong$ 79%, *cf.* Scheme 1) in the solid state as measured with an absolute photoluminescence quantum yield spectrometer (Quantaurus-QY, Hamamatsu). Herein, a blended powder of CBDAC and PPO was heated above the melting point of PPO on a heating stage and then the melt was cooled at a controlled rate with a lateral temperature gradient, which resulted in filmwise crystals of PPO doped with CBDAC (Fig. 1 and Section 1 of the ESI†). We identified the optimal mole ratio of CBDAC : PPO to be 1 : 30 000, which minimized the excitation threshold intensity (I_{th}) (Fig. S7, ESI†), used hereafter unless otherwise specified. Thus, only *ca.* 0.0033 mol% of CBDAC was dissolved in the melt liquid of PPO during the process described as follows.

We custom-designed and fabricated the processing apparatus (Fig. 1a and Fig. S1 of the ESI†). The main part of the apparatus consisted of a pair of stainless-steel (SUS) stages over which the same temperature gradients were formed. Each stage has two rod heaters embedded in the both ends, five thermocouples embedded between the heaters, and a heatsink attached to the cold end of the stage. We placed this setup in a vacuum chamber (Fig. S1, ESI†); the details regarding the apparatus are in Section 1.4 of the ESI.† Briefly, we sandwiched a blend of CBDAC and PPO (*ca.* 32 mg), placed inside a spacer ring (SUS, thickness: 200 μm, inner diameter: 8 mm), with two round glass substrates (EAGLE XG, Corning; diameter: 12 mm, thickness: 0.7 mm); we deposited the contacting surface to the SUS stage with a thin aluminum layer that served as a light reflector (Section 1.3 of the ESI†). During the process carried out under vacuum, we sealed the periphery of the stack with a perfluoroelastomer O-ring to prevent loss of the material, and we applied a compression force to the stack to ensure that the (i) O-ring was effective, (ii) resulting UC film had the same thickness as that of the spacer (Fig. 1a and Fig. S1, ESI†), and (iii) stage and substrate were in good thermal contact. We define ΔT as the difference between the temperatures measured with the two thermocouples at both ends separated by 24 mm (Fig. 1a and Fig. S2 of the ESI†). The minimum possible ΔT was 0.9 ± 0.4 °C because of the heatsink, which we denote "ΔT ~ 1 °C." We digitally controlled the temperature profile over the SUS stages such that it decreased at −3 °C min^{-1} (see Fig. S2 in the ESI† for the recorded changes of the temperature profiles). After the stack was taken out of the apparatus, the thin film was adhered to only one of the substrates because of the weaker adhesion of the film to the substrate than the integrity of the film. Thus, we performed all of the experiments in air; *i.e.*, with one surface of the film exposed to air. Before measurements, the film was annealed in dry nitrogen at 66 °C for 30 min for improving the crystallinity; previously, we found that annealing is important for crystalline UC solids.[17]

With ΔT ~ 1 °C, microcrystalline films with strong light scattering were generated (Fig. 2a, left), ascribed to a sudden solidification over the entire area. Notably, with ΔT = 20 °C, the film was comprised mostly of single-crystalline stripes grown along the temperature gradient (Fig. 2a, middle); the width of the stripes ranged mainly between 30 and 80 μm. We found some macroscopic cracks in the film, ascribed to the difference in the thermal expansion coefficients between the film and substrate. This result, which is highly reproducible, indicates a strong influence of the temperature gradient on the nature of the obtained film. The literature reports similar directional crystallization along the temperature gradient in films formed on a substrate from the melt of an organic p-type and n-type semiconductor blend.[21]

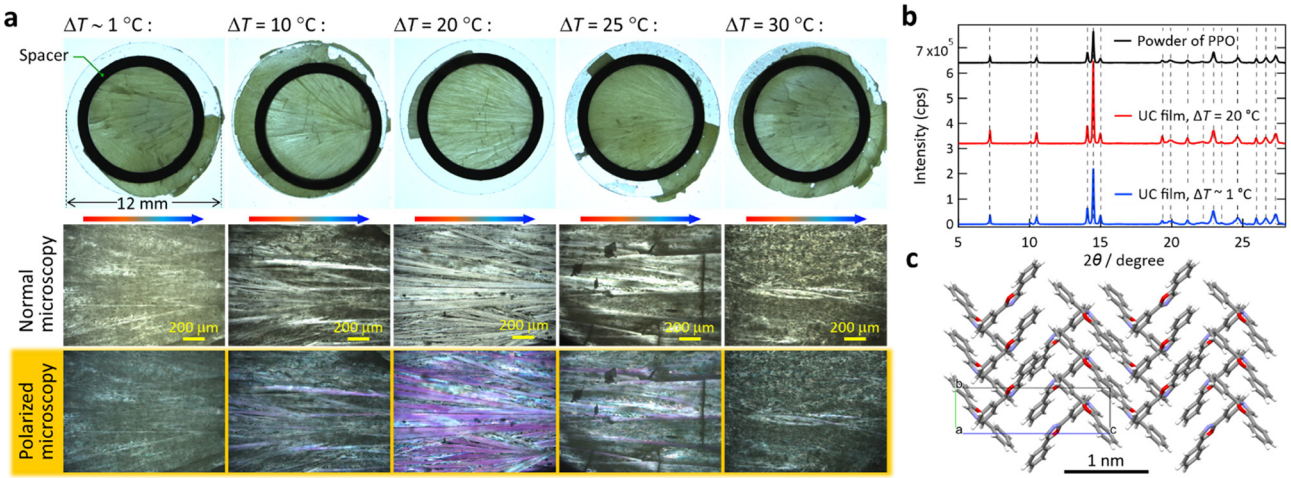

Fig. 2 Morphology and microscopic structure of the UC films prepared at CBDAC : PPO = 1 : 30 000 (in mol). (a) Digital photographs acquired with a stereo microscope (top) and magnified optical microscope images (bottom) of the samples prepared with various ΔT, all of which we acquired with transmitted illumination. In the polarized microscope images, crystalline domains were evident as purple-colored areas. (b) PXRD patterns acquired from the samples and as-received PPO powder, indicating the absence of polymorphism. (c) The crystal structure determined after Pawley and Rietveld refinements. See Section 6 of the ESI† for the results of the crystallographic analysis.

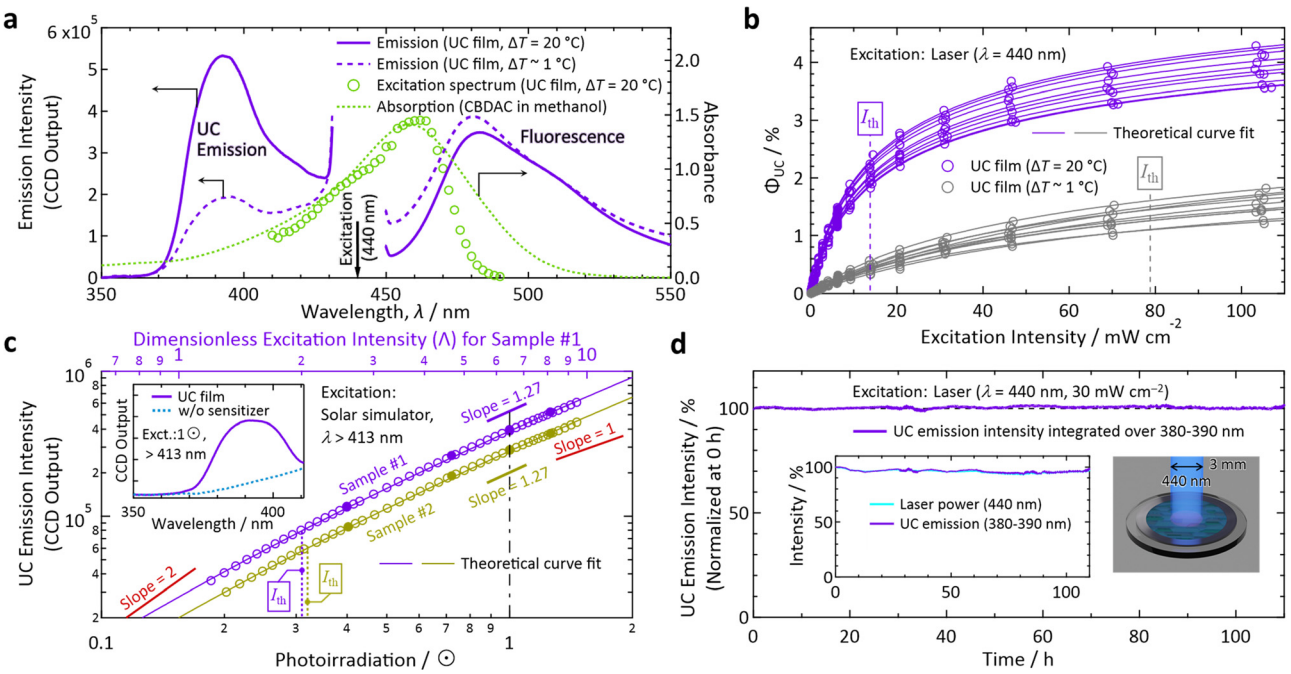

Fig. 3 Photoemission properties measured in air. (a) Spectra of emission from the films prepared with ΔT = 20 °C (solid curves) and ~ 1 °C (dashed curves) acquired with an incident laser light at λ = 440 nm. Also shown are an excitation spectrum (monitored at 380–390 nm) acquired with a wavelength-tunable laser from the film made with ΔT = 20 °C (circles) and an absorption spectrum of a methanol solution of CBDAC (dotted curve, 2 × 10^{-4} M, optical path length = 1 mm). (b) Dependence of Φ_{UC} on the intensity of excitation at 440 nm measured for samples prepared with ΔT = 20 °C (purple) and ~ 1 °C (gray), each of which we measured for 10 independently prepared samples. (c) Dependence of the UC emission intensity on the irradiance (in unit of sun, ⊙) of simulated sunlight, which passed through a λ > 413 nm long-pass filter placed above the sample (see Section 1.11 in the ESI†). Here, we measured two different samples #1 and #2, prepared with ΔT = 20 °C, to check the reproducibility. The inset shows the emission spectrum from the sample under 1 ⊙ irradiance (solid curve) and that from the reference prepared without the sensitizer (dotted curve). In panels (b) and (c), we first acquired the data represented by open marks by increasing the excitation light power, and then acquired the data represented by filled marks to confirm the reproducibility and sample stability. The theoretical fit curves used in panels (b) and (c) are eqn (35) and (36) of ref. 23, respectively. See eqn (28) and (29) of ref. 23 for details of the dimensionless excitation intensity Λ; Λ = 2 corresponds to I_{th}. (d) Test of photostability of the UC film prepared with ΔT = 20 °C by continuous irradiation of 440-nm laser light at an intensity of 30 mW cm^{-2} (see Fig. S3 in the ESI† for the setup). The vertical axis represents the UV–UC emission intensity corrected by the temporal fluctuation of the laser power shown in the inset.

Interestingly, when we increased ΔT to 25–30 °C, the films were again microcrystalline and highly opaque (Fig. 2a, right). This indicates that ΔT = 20 °C afforded an optimal moving speed of the solidification front line in a manner that facilitated growth of crystalline stripes. Aforementioned previous work also reported an optimal cooling rate, in which both too-slow and too-fast cooling rates perturbed the directional growth.[21] Although the report did not provide an explanation,[21] we confirmed this aspect by conducting a supporting experiment; use of a lower cooling rate of −1 °C min^{-1} with ΔT = 20 °C yielded similarly microcrystalline films (Fig. S8, ESI†). The UC films exhibited the same powder X-ray diffraction (PXRD) pattern as that of as-supplied PPO (Fig. 2b), indicating an absence of polymorphs. The Pawley and Rietveld refinements[22] indicate herringbone packing of PPO (Fig. 2c and Section 6 in the ESI†).

Hereafter, the photophysical properties are shown (Fig. 3; see Section 1 of the ESI† for experimental details). All I_{th} values were determined by fitting experimental data with eqn (35) or (36) of ref. 23. By irradiating the film with a laser light at a wavelength (λ) of 440 nm (diameter: 3 mm, beam profile: top hat, Fig. S3 in the ESI†), we observed an UC emission peaked at 390–393 nm with maximum fluorescence from CBDAC at 480–490 nm (Fig. 3a). The UC fluorescence was substantially redshifted compared with the fluorescence of PPO in solution (see Fig. S10, ESI† for absorption and emission spectra in dilute solutions). The UC emission from the sample prepared with ΔT = 20 °C was more intense than that prepared with $\Delta T \sim 1$ °C, ascribed to the higher crystallinity of the former (Fig. 2a). This explanation is supported by the *ca.* 2 × longer decay time-constant of the UC emission intensity for the former than the latter (Fig. S11, ESI†). The emission intensity distribution along the temperature-gradient direction was highly uniform (Fig. S13, ESI†), indicating that the crystals in this report were solid solutions similar to the crystals in our previous report.[17]

Because we determined the $\Phi_{F(S)}$ (*cf.* Scheme 1) of the UC film to be 5.1 ± 0.23% (0.23%: standard deviation for measurements on five different samples) with an absolute photoluminescence quantum yield spectrometer, Φ_{UC} could be determined by referencing to the fluorescence intensity; see Section 1.10 of the ESI† for details of the determination of Φ_{UC}. Herein, we define photoemission ranging in $\lambda \leq 425$ nm as UC emission. With this definition, 60.1% of the UC photons from the sample prepared with ΔT = 20 °C were UV photons with $\lambda < 400$ nm. The samples made with ΔT = 20 °C exhibited much higher efficiency (up to Φ_{UC} = 4.3% and η_{UC} = 8.6%) and a lower I_{th} than those made with $\Delta T \sim 1$ °C (Fig. 3b).

The I_{th} values for the cases of ΔT = 20 °C and $\Delta T \sim 1$ °C, from measurements of 10 different samples each, ranged over 13.8–17.0 and 78.8–93.5 mW cm^{-2}, respectively. In Fig. 3b, the minimum values are indicated. The aluminum light reflector deposited on the backside of the substrate decreased I_{th} by *ca.* 40%. Owing to the reflector, despite the low concentration of CBDAC (*ca.* 0.0033 mol% ≅ 1.92 × 10^{-4} M) in the PPO crystals, the absorptance by CBDAC in the film at 440 nm was *ca.* 61%, from which the excitation rate (k_{ex} in ref. 23) and excitation density (ex in ref. 24) of CBDAC at I_{th} are found to be *ca.* 7.7 × 10^{-4} M s^{-1} and *ca.* 2 × 10^{16} s^{-1} cm^{-2}, respectively (see Section 11 of the ESI† for these derivations). The emission intensities were maximal when the polarization direction of the incident laser light matched the direction of the crystal growth, whereas the intensity ratio of the UC fluorescence to CBDAC fluorescence was independent of the incident light polarization (Section 10, ESI†).

Notably, the value of I_{th} for sunlight irradiation cannot be determined from the value of I_{th} obtained by monochromatic excitation.[17,24] Therefore, we used broadband light generated with a solar simulator, which consisted only of the wavelength range of $\lambda > 413$ nm obtained with a long-pass filter (see Section 1.11 in the ESI† for details), representing the intensity in unit of suns (⊙). As shown in Fig. 3c for two samples prepared with ΔT = 20 °C (samples #1 and #2), the values of I_{th} were *ca.* 0.3 ⊙, indicating that the developed materials can be used for sunlight without concentration optics. These I_{th} values are reliable because the slope changed from *ca.* 1.6 to *ca.* 1.2, which is sufficient to perform theoretical curve fitting, and the vertical-axis values of Fig. 3c were highly reproducible (see the figure caption). We note that aforementioned annealing has improved Φ_{UC} by *ca.* 38% and decreased I_{th} by *ca.* 34% for samples prepared with ΔT = 20 °C (Fig. S15, ESI†) whereas the appearance of the films did not change.

To test the photostability, we irradiated the sample with laser light at λ = 440 nm at an intensity of 30 mW cm^{-2}, which was well above I_{th} (*cf.* Fig. 3b). Despite the fact that we carried out this test in air, the sample exhibited an outstanding photostability of >100 h (Fig. 3d), which is the longest record of photostability ever reported for TTA–UC to the best of our knowledge.

Finally, we exemplify a utility of this material. As graphically indicated in Fig. 4a, we applied a small quantity of UV-curing resin (BD-SKCJ, Bondic) to the mouth of two empty glass vials (outer diameter: 8 mm, height: 35 mm) and placed a glass slide onto them. Then, on the position of each vial's mouth, we placed the substrate on which the film was made with ΔT = 20 °C with and without including the sensitizer, termed "UC film" and "reference," respectively. After 3 min irradiation of 1 ⊙ light from the solar simulator with a $\lambda > 413$ nm

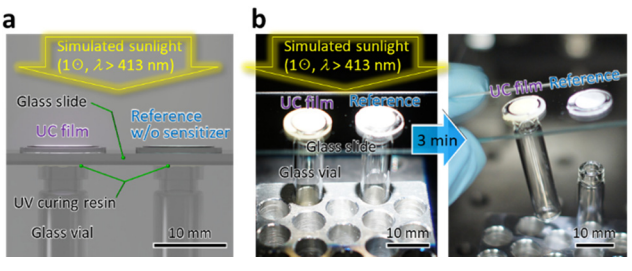

Fig. 4 (a) Schematic and (b) results of the demonstration of a utility of the UV–UC film applied to a solidification of UV curing resin with visible light ($\lambda > 413$ nm) of 1 ⊙ intensity at the sample position. Samples used here did not have a reflection aluminum layer on the bottom side.

long-pass filter, only the vial placed under the UC film was bonded to the glass slide, whereas that placed under the reference was not (Fig. 4b); we have confirmed reproducibility of this result. This demonstration conducted in air indicates a practical utility of the UV–UC films developed in this work.

Conclusions

For the first time, we created polycrystalline UV–UC films exhibiting a record-long photostability (>100 h), subsolar excitation threshold (*ca.* 0.3 ⊙), and high efficiency (up to Φ_{UC} = 4.3% and η_{UC} = 8.6%) in air by a solvent-free method that used a controlled temperature gradient. We revealed the impact of ΔT on the film properties and elucidated an essential importance of optimizing the temperature profile as well as the cooling speed. This novel class of UV-light-generating materials will substantially broaden the utility of ubiquitous terrestrial sunlight towards the extensive domain of UV-light-necessitating areas.

Author contributions

Y. M. conceived the idea and led this project. R. E. and Y. M. designed and developed the apparatus. R. E. conducted all of the experiments. Both authors wrote the manuscript and agreed with this submission.

Conflicts of interest

There are no conflicts to declare.

Acknowledgements

This work was financially supported by JSPS KAKENHI Grant Numbers JP17H03183 and JP20H02082 (Y. M.).

Notes and references

‡ Low crystallinity of organic UC solids was often resulted from the use of rapid solidification (or kinetically controlled) approaches, which were used to mitigate aggregation of the sensitizer species during formation of bicomponent organic solids.[7,16] See our previous paper[17] for detailed discussion on this point.

1 T. Takata, J. Jiang, Y. Sakata, M. Nakabayashi, N. Shibata, V. Nandal, K. Seki, T. Hisatomi and K. Domen, *Nature*, 2020, **581**, 411; H. Nishiyama, T. Yamada, M. Nakabayashi, Y. Maehara, M. Yamaguchi, Y. Kuromiya, Y. Nagatsuma, H. Tokudome, S. Akiyama, T. Watanabe, R. Narushima, S. Okunaka, N. Shibata, T. Takata, T. Hisatomi and K. Domen, *Nature*, 2021, **598**, 304; Y. Fang, Y. Hou, X. Fu and X. Wang, *Chem. Rev.*, 2022, **122**, 4204; H. Song, S. Luo, H. Huang, B. Deng and J. Ye, *ACS Energy Lett.*, 2022, **7**, 1043.

2 Y. Xu, S. Wang, J. Yang, B. Han, R. Nie, J. Wang, J. Wang and H. Jing, *Nano Energy*, 2018, **51**, 442; J. Low, B. Dai, T. Tong, C. Jiang and J. Yu, *Adv. Mater.*, 2019, **31**, 1802981; A. Behera, A. K. Kar and R. Srivastava, *Mater. Horiz.*, 2022, **9**, 607.

3 G. Barroso, Q. Li, R. K. Bordia and G. Motz, *J. Mater. Chem. A*, 2019, **7**, 1936; H. Samadian, H. Maleki, Z. Allahyari and M. Jaymand, *Coord. Chem. Rev.*, 2020, **420**, 213432.

4 M. Raeiszadeh and B. Adeli, *ACS Photonics*, 2020, **7**, 2941.

5 National Renewable Energy Laboratory, Reference Air Mass 1.5 Spectra, ASTM G–173–03, **https://www.nrel.gov/grid/solar-resource/spectra-am1.5.html**, accessed on October 22, 2022.

6 S. Baluschev, T. Miteva, V. Yakutkin, G. Nelles, A. Yasuda and G. Wegner, *Phys. Rev. Lett.*, 2006, **97**, 143903; T. N. Singh-Rachford and F. N. Castellano, *Coord. Chem. Rev.*, 2010, **254**, 2560; V. Gray, D. Dzebo, M. Abrahamsson, B. Albinsson and K. Moth-Poulsen, *Phys. Chem. Chem. Phys.*, 2014, **16**, 10345; T. F. Schulze and T. W. Schmidt, *Energy Environ. Sci.*, 2015, **8**, 103; P. Bharmoria, H. Bildirir and K. Moth-Poulsen, *Chem. Soc. Rev.*, 2020, **49**, 6529; A. Vasilev, R. Dimitrova, M. Kandinska, K. Landfester and S. Baluschev, *J. Mater. Chem. C*, 2021, **9**, 7119; J. K. Gallaher, K. M. Wright, L. Frazer, R. W. MacQueen, M. J. Crossley, F. N. Castellano and T. W. Schmidt, *Energy Environ. Sci.*, 2021, **14**, 5541; F. Edhborg, A. Olesund and B. Albinsson, *Photochem. Photobiol. Sci.*, 2022, **21**, 1143.

7 A. Monguzzi, R. Tubino, S. Hoseinkhani, M. Campione and F. Meinardi, *Phys. Chem. Chem. Phys.*, 2012, **14**, 4322.

8 T. N. Singh-Rachford and F. N. Castellano, *J. Phys. Chem. A*, 2009, **113**, 5912.

9 M. Majek, U. Faltermeier, B. Dick, R. Pérez-Ruiz and A. J. von Wangelin, *Chem. – Eur. J.*, 2015, **21**, 15496; H. L. Lee, M. S. Lee, H. Park, W. S. Han and J. H. Kim, *Korean J. Chem. Eng.*, 2019, **36**, 1791; Y. Murakami, A. Motooka, R. Enomoto, K. Niimi, A. Kaiho and N. Kiyoyanagi, *Phys. Chem. Chem. Phys.*, 2020, **22**, 27134; A. Olesund, J. Johnsson, F. Edhborg, S. Ghasemi, K. Moth-Poulsen and B. Albinsson, *J. Am. Chem. Soc.*, 2022, **144**, 3706; T. J. B. Zähringer, M. S. Bertrams and C. Kerzig, *J. Mater. Chem. C*, 2022, **10**, 4568; Y. Wei, K. Pan, X. Cao, Y. Li, X. Zhou and C. Yang, *CCS Chem.*, 2022, **4**, 3852.

10 N. Harada, Y. Sasaki, M. Hosoyamada, N. Kimizuka and N. Yanai, *Angew. Chem., Int. Ed.*, 2021, **60**, 142.

11 M. Uji, N. Harada, N. Kimizuka, M. Saigo, K. Miyata, K. Onda and N. Yanai, *J. Mater. Chem. C*, 2022, **10**, 4558.

12 P. Duan, N. Yanai and N. Kimizuka, *Chem. Commun.*, 2014, **50**, 13111; N. Yanai, M. Kozue, S. Amemori, R. Kabe, C. Adachi and N. Kimizuka, *J. Mater. Chem. C*, 2016, **4**, 6447; V. Gray, P. Xia, Z. Huang, E. Moses, A. Fast, D. A. Fishman, V. I. Vullev, M. Abrahamsson, K. Moth-Poulsen and M. L. Tang, *Chem. Sci.*, 2017, **8**, 5488; M. Barawi, F. Fresno, R. Pérez-Ruiz and V. A. de la Pena O'Shea, *ACS Appl. Energy Mater.*, 2019, **2**, 207; S. He, X. Luo, X. Liu, Y. Li and K. Wu, *J. Phys. Chem. Lett.*, 2019, **10**, 5036; B. Pfund, D. M. Steffen, M. R. Schreier, M. S. Bertrams, C. Ye, K. Börjesson, O. S. Wenger and C. Kerzig, *J. Am. Chem. Soc.*, 2020, **142**, 10468; L. Hou, A. Olesund, S. Thurakkal, X. Zhang and B. Albinsson, *Adv. Funct. Mater.*, 2021, **31**, 2106198; X. Lin, Z. Chen, Y. Han, C. Nie, P. Xia, S. He, J. Li and K. Wu, *ACS Energy Lett.*, 2022, **7**, 914.

13 P. E. Keivanidis, S. Baluschev, T. Miteva, G. Nelles, U. Scherf, A. Yasuda and G. Wegner, *Adv. Mater.*, 2003, **15**, 2095; S. Baluschev, P. E. Keivanidis, G. Wegner, J. Jacob, A. C. Grimsdale and K. Müllen, *Appl. Phys. Lett.*, 2005, **86**, 061904; R. R. Islangulov, J. Lott, C. Weder and F. N. Castellano, *J. Am. Chem. Soc.*, 2007, **129**, 12652; A. Monguzzi, R. Tubino and F. Meinardi, *J. Phys. Chem. A*, 2009, **113**, 1171; T. N. Singh-Rachford, J. Lott, C. Weder and F. N. Castellano, *J. Am. Chem. Soc.*, 2009, **131**, 12007; Y. C. Simon and C. Weder, *J. Mater. Chem.*, 2012, **22**, 20817.

14 P. B. Merkel and J. P. Dinnocenzo, *J. Lumin.*, 2009, **129**, 303.

15 M. Wu, D. N. Congreve, M. W. B. Wilson, J. Jean, N. Geva, M. Welborn, T. V. Voorhis, V. Bulović, M. G. Bawendi and M. A. Baldo, *Nat. Photonics*, 2016, **10**, 31; V. Gray, K. Moth-Poulsen, B. Albinsson and M. Abrahamsson, *Coord. Chem. Rev.*, 2018, **362**, 54; B. Joarder, N. Yanai and N. Kimizuka, *J. Phys. Chem. Lett.*, 2018, **9**, 4613; K. M. Felter, M. C. Fravventura, E. Koster, R. D. Abellon, T. J. Savenije and F. C. Grozema, *ACS Energy Lett.*, 2020, **5**, 124; S. Izawa and M. Hiramoto, *Nat. Photonics*, 2021, **15**, 895; J. Alves, J. Feng, L. Nienhaus and T. W. Schmidt, *J. Mater. Chem. C*, 2022, **10**, 7783; S. E. Seo, H. S. Choe, H. Cho, H. Kim, J. H. Kim and O. S. Kwon, *J. Mater. Chem. C*, 2022, **10**, 4483; L. Wei, C. Fan, M. Rao, F. Gao, C. He, Y. Sun, S. Zhu, Q. He, C. Yang and W. Wu, *Mater. Horiz.*, 2022, **9**, 3048.

16 S. H. Lee, J. R. Lott, Y. C. Simon and C. Weder, *J. Mater. Chem. C*, 2013, **1**, 5142; R. Vadrucci, C. Weder and Y. C. Simon, *J. Mater. Chem. C*, 2014, **2**, 2837; R. Karpicz, S. Puzinas, V. Gulbinas, A. Vakhnin, A. Kadashchuk and B. P. Rand, *Chem. Phys.*, 2014, **429**, 57; H. Goudarzi and P. E. Keivanidis, *J. Phys. Chem. C*, 2014, **118**, 14256; M. Hosoyamada, N. Yanai, T. Ogawa and N. Kimizuka, *Chem. – Eur. J.*, 2016, **22**, 2060; S. Raišys, K. Kazlauskas, S. Juršėnas and Y. C. Simon, *ACS Appl. Mater. Interfaces*, 2016, **8**, 15732; K. Kamada, Y. Sakagami, T. Mizokuro, Y. Fujiwara, K. Kobayashi, K. Narushima, S. Hirata and M. Vacha, *Mater. Horiz.*, 2017, **4**, 83; K. Kamada, Y. Sakagami, T. Mizokuro, Y. Fujiwara, K. Kobayashi, K. Narushima, S. Hirata and M. Vacha, *Mater. Horiz.*, 2018, **5**, 1219(correction); H. Goudarzi and P. E. Keivanidis, *ACS Appl. Mater. Interfaces*, 2017, **9**, 845; T. Ogawa, M. Hosoyamada, B. Yurash, T. Q. Nguyen, N. Yanai and N. Kimizuka, *J. Am. Chem. Soc.*, 2018, **140**, 8788; T. Ogawa, N. Yanai, H. Kouno and N. Kimizuka, *J. Photonics Energy*, 2018, **8**, 022003; A. Abulikemu, Y. Sakagami, C. Heck, K. Kamada, H. Sotome, H. Miyasaka, D. Kuzuhara and H. Yamada, *ACS Appl. Mater. Interfaces*, 2019, **11**, 20812; E. M. Rigsby, T. Miyashita, D. A. Fishman, S. T. Roberts and M. L. Tang, *RSC Adv.*, 2021, **11**, 31042; S. Raišys, O. Adomėnienė, P. Adomėnas, A. Rudnick, A. Köhler and K. Kazlauskas, *J. Phys. Chem. C*, 2021, **125**, 3764; N. Tripathi, M. Ando, T. Akai and K. Kamada, *J. Mater. Chem. C*, 2022, **10**, 4563.

17 R. Enomoto, M. Hoshi, H. Oyama, H. Agata, S. Kurokawa, H. Kuma, H. Uekusa and Y. Murakami, *Mater. Horiz.*, 2021, **8**, 3449.

18 X. Jiang, X. Guo, J. Peng, D. Zhao and Y. Ma, *ACS Appl. Mater. Interfaces*, 2016, **8**, 11441.

19 D. P. Specht, P. A. Martic and S. Farid, *Tetrahedron*, 1982, **38**, 1203.

20 D. Huang, J. Sun, L. Ma, C. Zhang and J. Zhao, *Photochem. Photobiol. Sci.*, 2013, **12**, 872.

21 G. Liu, J. Liu, A. S. Dunn, P. Nadazdy, P. Siffalovic, R. Resel, M. Abbas, G. Wantz and Y. H. Geerts, *Cryst. Growth Des.*, 2021, **21**, 5231.

22 H. M. Rietveld, *Acta Crystallogr.*, 1967, **22**, 151; G. S. Pawley, *J. Appl. Crystallogr.*, 1981, **14**, 357.

23 Y. Murakami and K. Kamada, *Phys. Chem. Chem. Phys.*, 2021, **23**, 18268.

24 Y. Zhou, F. N. Castellano, T. W. Schmidt and K. Hanson, *ACS Energy Lett.*, 2020, **5**, 2322.